33RD CONGRESS
OF THE INTERNATIONAL COUNCIL
OF THE AERONAUTICAL SCIENCES
STOCKHOLM, SWEDEN, 4–9 SEPTEMBER, 2022

ICAS 2022 SWEDEN

RESEARCH ON PRESSURE LOAD OF AN EMBEDDED JET NOZZLE

Li Hongyang*, Wang Xiao, Yu Dongsheng, Liu Fangliang

Shenyang Aircraft Design and Research Institute, Shenyang, 110035, China.

1. Introduction

Embedded nozzle can greatly improve the stealth performance of aircraft, such as the design of RQ-180 and X-47B, while it also brings new challenges to aircraft design, especially in the fields of aerodynamics and aerodynamic load.

From the aerodynamic point of view, the aircraft after-body is faced with complex and harsh load environment, such as strong pulsation effect of high temperature and high pressure engine jet, the coupling of effect of aerodynamic load and thermal load, the shock wave/boundary layer interaction, the complex shear and mixing of multiple streams, etc. The complex flow phenomenon makes it difficult to predict the aerodynamic load of the after-body. From the open-published literature, there are few researches on the mechanism of dynamic load coursed by jet mixing.

In the published literature, there is relatively little research on the embedded nozzle, especially on the study of aerodynamic load. Bridges[1] design a family of high aspect ratio nozzles to provide a parametric database of canonical embedded propulsion concepts, and CFD simulations were made to predict the thrust performance and to optimize parameters. Wang[2] introduces the multi-S curved nozzle, two-dimensional nozzle and ejector nozzle into the design of the embedded nozzle, and conducted some analysis. Lin and Wang[3] analyzes the role of nozzle in different stages of development of integrated design technology for flight and engine, and introduces the problems that should be considered in nozzle design in different stages of development. Mohan & Dowling[4] used the prediction method based on RANS to parametrically study the effects of different sawtooth numbers, sawtooth entry angles and micro jet injection angles on the design of jet noise reduction.

Many researchers have used experimental methods to study the jet aerodynamic phenomenon, mainly are combined with the noise test. Gee[5] designed a three-dimensional sound intensity sensor, which is mainly composed of a sound pressure sensor and three mutually orthogonal particle vibration velocity sensors. Gee used the designed sound intensity sensor to measure the near-field sound intensity of small solid rocket motor. Using a similar method, Gee et al.[5] measured the near sound field of jet noise of F-22 Raptor fighter is analyzed, and the variation of aerodynamic noise spectrum from near field to far field is analyzed. Chu and Kaplan [6] found that the main sound source area of high subsonic jet noise is located behind the core area downstream of the jet, and the sound source characteristics change with the change of velocity and radiation angle The turbulent kinetic energy of the sound source at the end of the core area is high, and the main noise source of the jet can be obtained by determining the location of the core area. Tam & Seine[7] and Viswanathan[8] further strongly proved that the high subsonic jet noise is mainly composed of two parts: one is the large-scale turbulent mixing noise that dominates in the downstream direction, and the other is the small-scale turbulence that dominates in the upstream and sideline directions. In 2007, Wernet[9] of NASA Glenn Research Center and others developed

and verified the high frequency response Particle Image Velocimetry (TRG-PIV) technology to meet the needs of acoustic research This technology is used to study the flow structure of cold/hot jets, including the attenuation of turbulent structure and the development of shear layer, which can effectively capture the development of jet shear layer and turbulent structure

In this paper, a simplified embedded nozzle of an UAV was taken as the research object, and the wind tunnel test and CFD simulation method was combined to analysis the steady and unsteady aerodynamic loads under the action of jet.

2. Research contents and methods

2.1 Research object

The research object is a simplified embedded nozzle, which is a little similar as the one shown in Fig.1 (download from Internet). The nozzle duct is round to oblate, with the shrinkage ratio of 0.35. The nozzle has an upper expansion edge and a lower expansion edge, of witch, the length of the lower one is 2.8 times of that of the upper one. The nozzle duct and the upper and lower expansion edges are sleeved installed, with a secondary flow gap of about 20 mm.

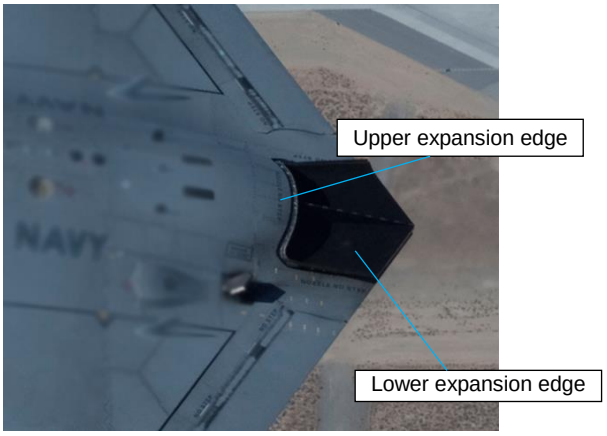

Fig.1 Typical embedded nozzle (X47B)

2.2 Wind tunnel test

The high-speed and low-speed wind tunnel test were conducted, mainly to obtain the jet effect force and the surface pressure data. The test section of the high speed wind tunnel is 1.5m, and that of the low speed win tunnel is 2.5m. In general, the measurement accuracy of the steady-state pressure sensor is better than 0.1% FS(Full Scale). The nozzle pressure ratio (NPR) was continuously adjustable. Both the steady-state pressure and dynamic press data were obtained, and the variation with the external flow Ma, NPR, and attack angle, sideslip angle was researched.

The dynamic test adopts the Kulite dynamic pressure sensor, the dynamic sampling frequency of the measurement section is set to 100kHz, the low-pass cut-off frequency is set to 5kHz, and the filter type is selected as FIR@-0.1dB DC coupling is selected for dynamic measurement.

The total pressure regulating range of jet is 0.02MPa~0.7 MPa, and the accuracy is better than 0.2% local value; The range of ambient pressure regulation is 0.02MPa~0.12MPa, and the pressure regulation accuracy is better than 0.20% FS(Full Scale); The range of PSI scanning valve is 0~+50PSI, 0~+150PSI, and the pressure measurement accuracy is 0.05%FS; The flowmeter range is 0.1kg/s~7.5kg/s; The measurement accuracy is 0.2% local value; The pressure scanning frequency of the pressure data acquisition system is 5000ch/s, the range is -15PSI~+30 PSI, and the pressure measurement accuracy is ± 0.03%FS.

2.3 CFD calculation

Three-dimensional integral Reynolds averaged N-S equations in Cartesian coordinate system.

$$\frac{\partial}{\partial t}\int_{\Omega} \boldsymbol{Q}\mathrm{d}\Omega + \oint_{\partial\Omega}\left(\boldsymbol{F}_c - \boldsymbol{F}_v\right)\cdot\boldsymbol{n}\mathrm{d}S = \int_{\Omega}\boldsymbol{S}\mathrm{d}\Omega$$

Where $\boldsymbol{Q}$ is the conserved quantity, $\boldsymbol{F}_c$ is the convective flux, $\boldsymbol{F}_v$ is the diffusive flux, $\boldsymbol{S}$ is the source term, Ω is the control volume, $\partial\Omega$ is the boundary of the control volume, and $\boldsymbol{n}$ is the normal vector pointing outward.

The finite volume method based on unstructured grid is used for spatial discretization, the ROE upwind scheme is used for convective flux discretization, and the central difference scheme is used for viscous flux discretization. The k-ω SST two-equation turbulence model is selected for stead-state calculation, which is solved based on the fully implicit time marching method.

The unsteady state calculation adopts IDDES method [10] based on k-ω SST turbulence model, which is a kind of RANS/LES hybrid method. It effectively combines the advantage of the two methods, and has been widely used because of its high accuracy and acceptable calculation consuming [11]. It can solve engineering problems such as boundary layer flow, mixing of primary and secondary flows in jet calculation.

The mixed grid is used for CFD calculation, and the jet region is approximated to a structured grid to obtain higher spatial resolution and calculation accuracy. Taking the equivalent diameter of the nozzle as a reference, the grid scale in the core area of the jet is about 1/100 of the equivalent diameter, and in the region around the fuselage is about 1/25 of the equivalent diameter. The wake region of the jet is multi encrypted to make it transition naturally with the grid of the far-field boundary. In the area near the wall, the prism layer is used for densification, and the height of the first layer of grid is about 5e-6 of the equivalent diameter of the nozzle. The total number of grids is about 60million. Spatial discretization has second-order accuracy. The time advance adopts the double time step method, which has second-order accuracy.

3. Results and analysis

3.1 Verification of steady-state results

Fig.2 shows the steady-state pressure distribution of the expansion edge under the condition of Ma=0.85, NPR=3.5. It can be seen that the alternating pressure and suction loads near the nozzle exit are relatively large, while the loads in the rear region decreases rapidly. Because of the mixing of the jet and the external flow, the strength of the shock waves and expansion waves get weaker gradually. The position of the red dotted line is the projection of the upper expansion edge. The contour indicates that the upper expansion edge could affect the pressure distribution on the lower expansion edge directly.

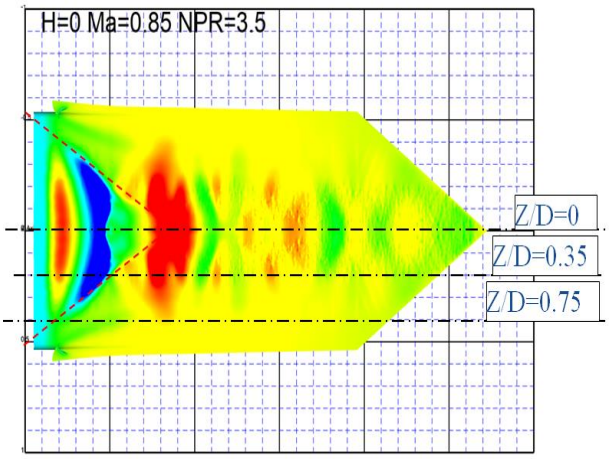

Fig.2 pressure distribution of lower expansion edge (Ma=0.85)

Fig.3 (a), (b)and(c) respectively shows the comparison between the calculated press distribution of different z cut-lines and the test data. The cut-lines are shown in Fig.2, where D is the width of the half-model expansion edge, and L is the length of the lower expansion edge. The z/D and x/L could represent the relative position. It can be seen that the fluctuation amplitude of pressure value decreases gradually with the increase of span-wise distance, and is almost uniform at z/D=0.75. In engineering application, a fluctuation threshold can be set to artificially delimit the range of jet influence area, to facilitate data processing. The calculated results are in good agreement with the test data, which proves the accuracy of the numerical calculation method.

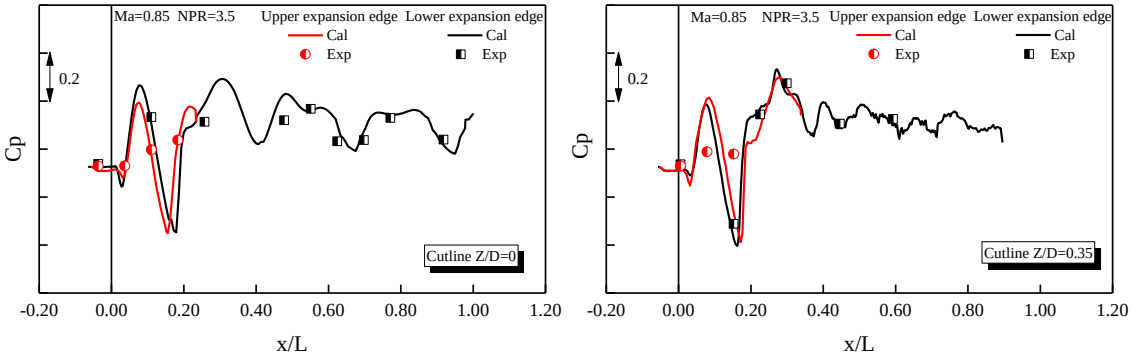

(a) Cutline Z/D=0

(b) Cutline Z/D=0.35

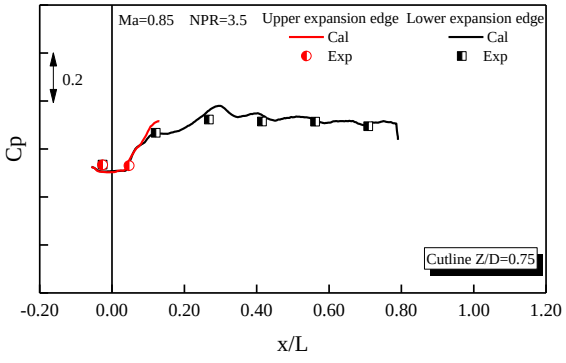

(c) Cutline Z/D=0.75

Fig.3 Comparison between the calculated results and the wind tunnel test results

3.2 Analysis of the unsteady jet flow field

Fig.4 (a), (b) show the comparison of between the steady-state pressure distribution and dynamic pressure distribution of the cross-section. The left part of in the figure is the outlet of the nozzle duct. The simulated condition is no external flow, NPR equals 2.7, and physical time step equals 1e-4 s.

The flow field is mainly divided into two regions, the jet core region and the mixing region. It can be seen that in the jet core region, the two results are a little similar, especially in the area near the outlet of the nozzle duct. In this area, the alternating change of pressure is mainly due to the distribution of shock waves and expansion waves.

While in the mixing region, there are big differences between the two results. The steady-state results cannot capture the shedding vortex caused by shear mixing, and the pressure distribution is almost uniform. It's because that the time averaged effect of positive pressure vortex and negative pressure vortex is "zero". Namely, the steady-state result could not reflect the real pressure load in the mixing region, quite a lot of the load information is neglected.

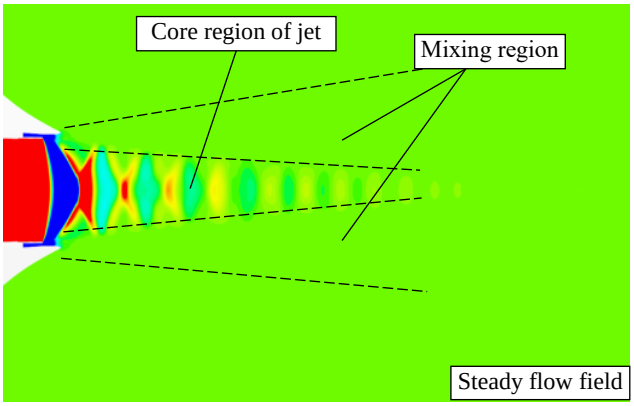

(a) steady flow field

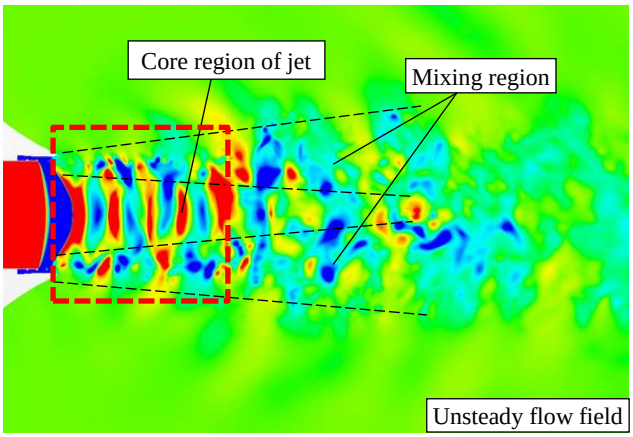

(b) unsteady flow field

Fig.4 Comparison of the steady and unsteady field on the cross section by CFD

As shown in Fig.5, as many as 260 dynamic pressure monitoring points are set on the wall of the lower expansion edge. Among which, 5 points (cyan bold ones) are corresponding to the both high speed and low speed wind tunnel test. All the dynamic pressure time-domain information of these monitoring points are recorded and processed in the frequency-domain information as PSD (Power Spectral Density, Pa2/Hz) or SPL(Sound Pressure Level, dB), or OASPL (Overall SPL, dB).

As shown in Fig.6, a cut-line at x/L=0.5 on the wall of the lower expansion edge was selected, to draw the distribution curve of the frequency-domain information along the crosswise direction.

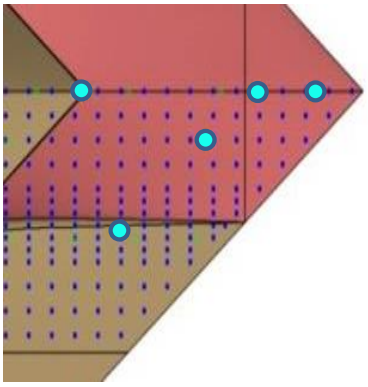

Fig.5 Layout of wall dynamic monitor points

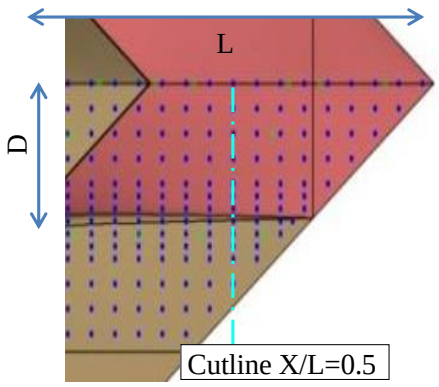

Fig.6 Layout of parameter processing cut-line

The wall pressure fluctuation under the action of jet flow is a random signal, which cannot be directly transformed by Fourier-Transfer, and cannot get the accurate power spectral density function in theory. It can only be approximated by limited sample data, so the result depends on the data processing method and the mathematical model of fitting. It is considered that the AR model [12-13], which is one of the modern spectral estimation methods, is suitable for the analysis of jet pressure fluctuation.

The dynamic aerodynamic loads on the expansion wall are measured in both high and low speed wind tunnel tests. The comparison between the calculated SPL and the test data are show in Fig. 5. It reveals that the calculated results are in good agreement with the test data, especially in the frequency range of 10Hz~1000Hz. The part higher than 1000Hz belongs to the category of noise, which is not the focus of aerodynamic load.

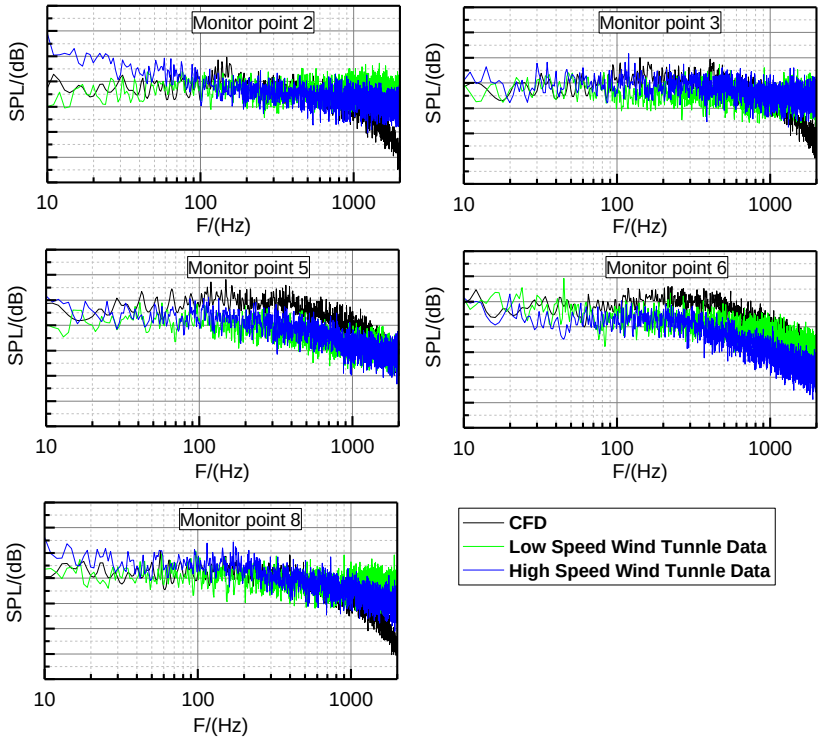

Fig.7 Comparison of the calculated SPL with the test data

Fig.8 shows the distributions of PSD on 11 monitoring points on the cut-line of X/L=0.5, which refers to Fig.6. It reveals that, along the crosswise, in the middle position, the PSD value is relatively low (point 1~4), and then rapidly increases (point 5~7), and then decreases to close to 0 (point8~11). It

seems that there is a narrow area that is with very high dynamic load. While, the dynamic load in other areas is relatively low. The dominant frequency range also increases, overall in 100Hz ~1000H.

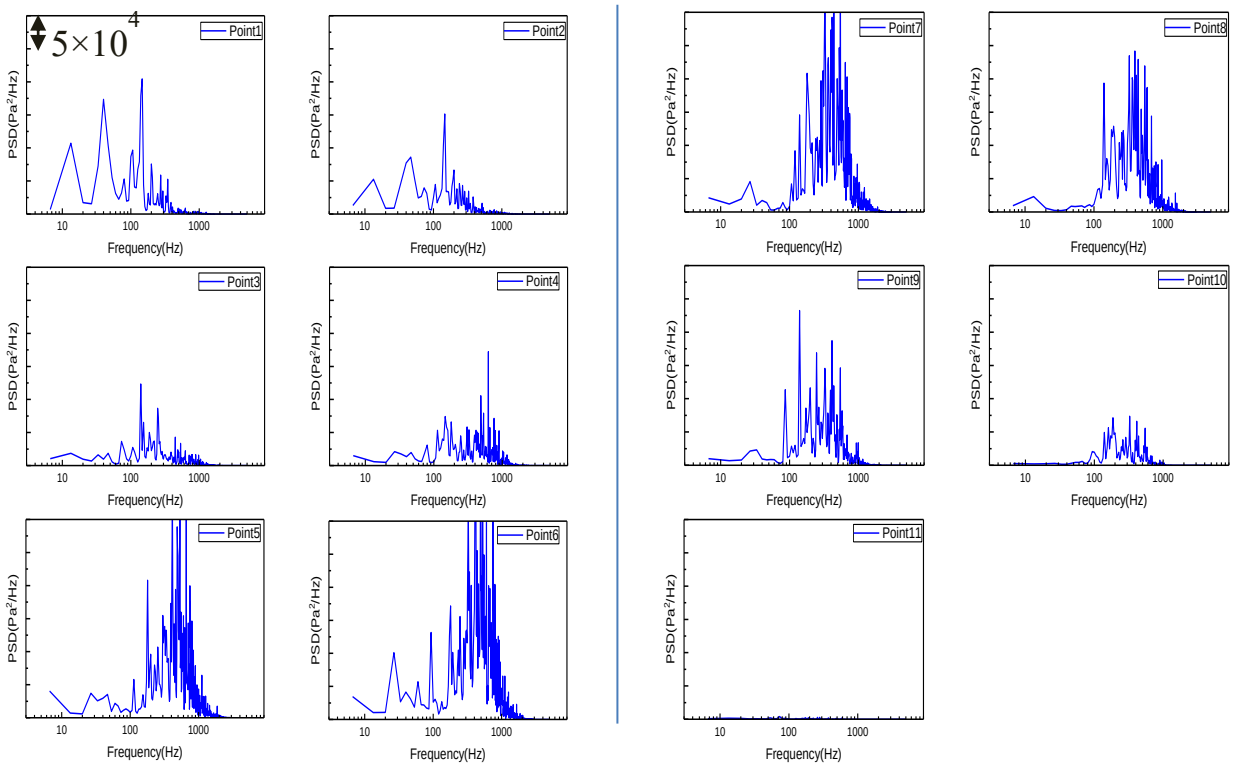

Fig.8 PSD of point1～point11, cutline X/L=0.5 (in Fig.6)

Fig.9 shows the contour of the overall sound pressure level (OASPL) on the lower expansion, which corresponds to the red box area in Fig. 3(b). The dot lines also correspond to the partition in Fig. 3(b). The parameter OASPL could reflect the level of dynamic pressure load.

It can be seen that the area with the largest dynamic pressure load locates at the mixing region of the jet and the external flow, while the steady-state pressure load in this area is relatively small, which should be analyzed together with Fig.4(a) and Fig.4(b).

In other words, the steady-state and dynamic pressure loads are formatted by different mechanisms. The steady-state pressure load is mainly formatted by the jet shock/expansion wave, while the dynamic pressure load is mainly formatted by the shear mixing of the jet and external flow. The factors related to the shock/expansion wave could affect the steady-state pressure load directly, such as NPR, ambient static pressure, and the wall surface shape. While, the influence factors of the dynamic pressure load is much more complicated, and more difficult to calculate.

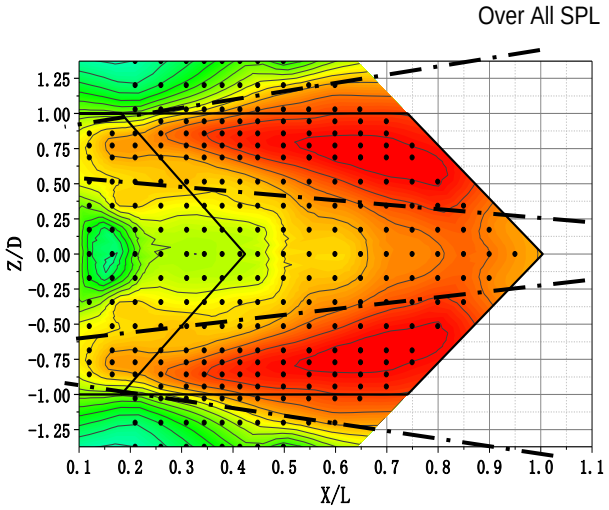

Fig.9 Distribution of the strength of the dynamic pressure load (OASPL)

4. Conclusions

A simplified embedded nozzle was taken as the research object; steady and dynamic pressure load was studied by CFD. Conclusions are as follows:

(1) On the both upper and lower expansion edges, the steady pressure load are positive and negative alternated, affected by NPR, and the extremum value occurs at the core region of jet flow, especially near the nozzle outlet;

(2) The steady CFD method could get accurate results compared with wind tunnel data, while, it cannot obtain the mixing phenomenon of the jet and the external flow; In other words, it can only give the steady-state aerodynamic load, while the dynamic aerodynamic load is ignored;

(3) Different from the steady pressure load, the extemum of dynamic pressure load occurs at the boundary region of the jet flow (where the steady pressure load is relatively low). It is mainly coursed by shear layer mixing between core jet flow and the external flow.

5. Copyright Statement

References

[1] Bridges J E . Noise of Embedded High Aspect Ratio Nozzles[C]// *2011 Technical Conference Fundamental Aeronautics Program*. 2011.

[2] Wang J Q, Fang L, Kong D Y. A Preliminary Investigation of Multi-S Shaped 2D Eject-nozzle Design [J]. *Aircraft Engineering*, 2010(1):4. (in Chinese)

[3] Lin P, Wang D. Function of Nozzle in Integrated Design of Aircraft and Engines[J]. *Aero Weaponry*, 2021, 28(4):1-6. (in Chinese)

[4] Mohan N K. Depuru and Dowling A P. Jet-noise-prediction model for chevrons and micro jets [J]. *AIAA Journal*, 2016, 54 (12): 3928-3940.

[5] Gee K L, Giraud J H, Blotter J D, et al. Near-field vector intensity measurements of a small solid rocket

motor[J]. *Journal of the Acoustical Society of America*, 2010, 128(2): EL69.

[6] Chu W T, Kaplan R E. Use of a spherical concave reflector for jet-noise source distribution diagnosis [J]. *Journal of the Acoustical Society of America*, 1976, 59(6): 1268-1277.

[7] Tam C K W, Golebiowski M, Seiner J M. On the two components of turbulent mixing noise from supersonic jets [R]. *AIAA* 1996-1716.

[8] Viswanathan K. Analysis of the two similarity components of turbulent mixing noise [J]. *AIAA Journal*, 2002, 40(9): 1735-1744.

[9] Wernet M P. Temporally resolved PIV for space-time correlations in both cold and hot jet flows [J]. *Measurement Science and Technology*, 2007, 18(5): 1387-1403

[10]Xiao L H, Xiao Z X, Duan Z W, etal. Improved-delayed-detached-eddy simulation of cavity-induced transition in hypersonic boundary layer [J]. *International Journal of Heat and Fluid Flow*, 2015, 51: 138-150.

[11]Spalart P R. Detached-eddy simulation [J]. *Annual Review of Fluid Mechanics*, 2009, 41: 181-202.

[12]LIU X Y, HU H Y, WU S, et al. Performance analysis on spectrum resolution ratio and small noise-signal ratio of ar model-based power spectrum estimation [J]. *Ship Electronic Engineering*, 2018, 38(7): 126-131(in Chinese).

[13]LIU M X, WANG X G. Performance analysis on spectrum resolution ratio and small noise-signal ratio of AR model-based power spectrum estimation [J]. *Electronic Design Engineering*, 2017, 25(17): 129-132(in Chinese).

Contact Author Email Address

Name: Li Hongyang

E-mail: lihongyang601@126.com